4 Reaction Pathways of Alkoxy radicals

4.1 Introduction

Volatile organic hydrocarbons (VOCs) are released into the atmosphere in large quantities from both anthropogenic and biogenic sources. Once in the troposphere, VOCs are degraded through oxidation initiated by reaction with radicals or photolysis. In these oxidative processes, alkoxy radicals (RO) are often a key intermediate that can react further via one of several mechanisms. The branching ratios of the various pathways determine the distribution of final oxidation products, and therefore impact the extent to which emitted VOCs contribute to the formation of ozone, smog, and secondary organic aerosols.

The oxidation of alkanes (denoted RH here) provides the simplest example of alkoxy radical chemistry. In the presence of NO_x, alkoxy radicals are formed from alkanes in the troposphere predominantly by the following mechanism:

$$RH + \bullet OH \longrightarrow R\bullet + H_2O, \qquad \text{Reaction 4.1}$$

$$R\bullet + O_2 \xrightarrow{M} RO_2\bullet, \qquad \text{Reaction 4.2}$$

$$RO_2\bullet + NO \longrightarrow RO\bullet + NO_2. \qquad \text{Reaction 4.3}$$

The NO_2 formed in this process undergoes photolysis in the troposphere (<425 nm) to yield O atoms that subsequently react with O_2 to generate ozone. Alkoxy radicals react further via one of three mechanisms: α-hydrogen abstraction by O_2 to form a carbonyl and HO_2, unimolecular isomerization involving a 1,5-hydrogen shift via a cyclic

transition state, or unimolecular dissociation via β-scission. These three reactions for the *n*-butoxy radical (a primary alkoxy radical) and the 2-pentoxy radical (a secondary alkoxy radical) are shown below.

n-butoxy: O_2

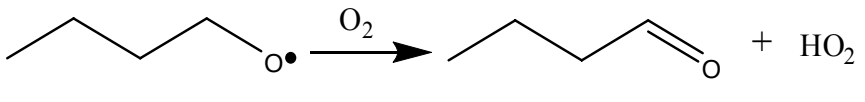

Reaction 4.4

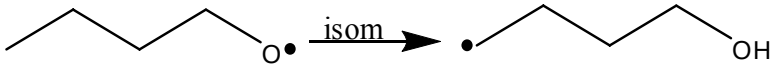

Reaction 4.5

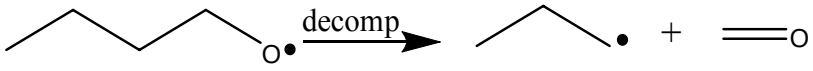

Reaction 4.6

2-pentoxy:

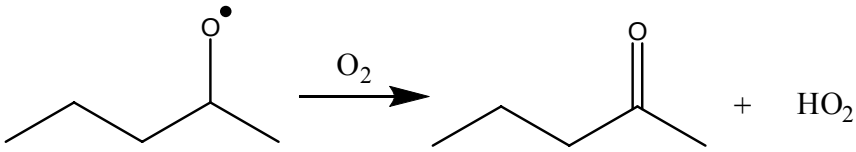

Reaction 4.7

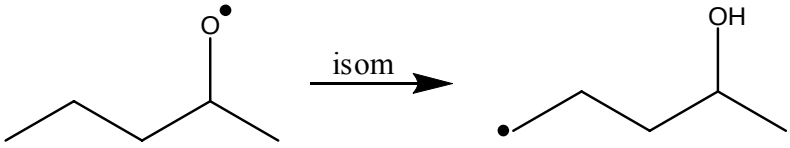

Reaction 4.8

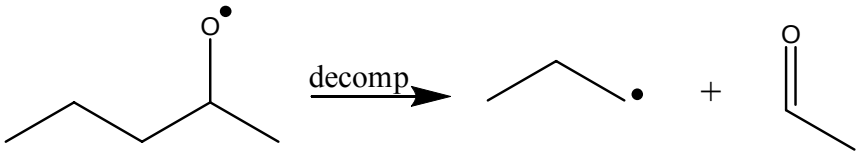

Reaction 4.9

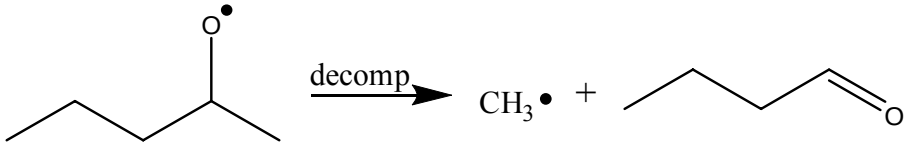

Reaction 4.10

The potential energy surface over which these reactions proceed for the *n*-butoxy radical is shown in Figure 4.1. The branching ratio for each of these pathways depends critically upon the structure of the alkoxy radical. All alkoxy radicals containing an α-hydrogen can undergo reaction with O_2. While the rate constant for reaction with O_2, k_{O2}, has been observed to vary slightly with temperature and the structure of the alkoxy radical, measurements of k_{O2} have generally yielded values within a factor of two of 1×10^{-14} cm^3 $molec^{-1}$ s^{-1} at 298 K [77, 78]. Variations in k_{isom} and k_{decomp} with pressure, temperature, and molecular structure are much larger, spanning many orders of magnitude because of the significant barriers involved and differences in the densities of states.

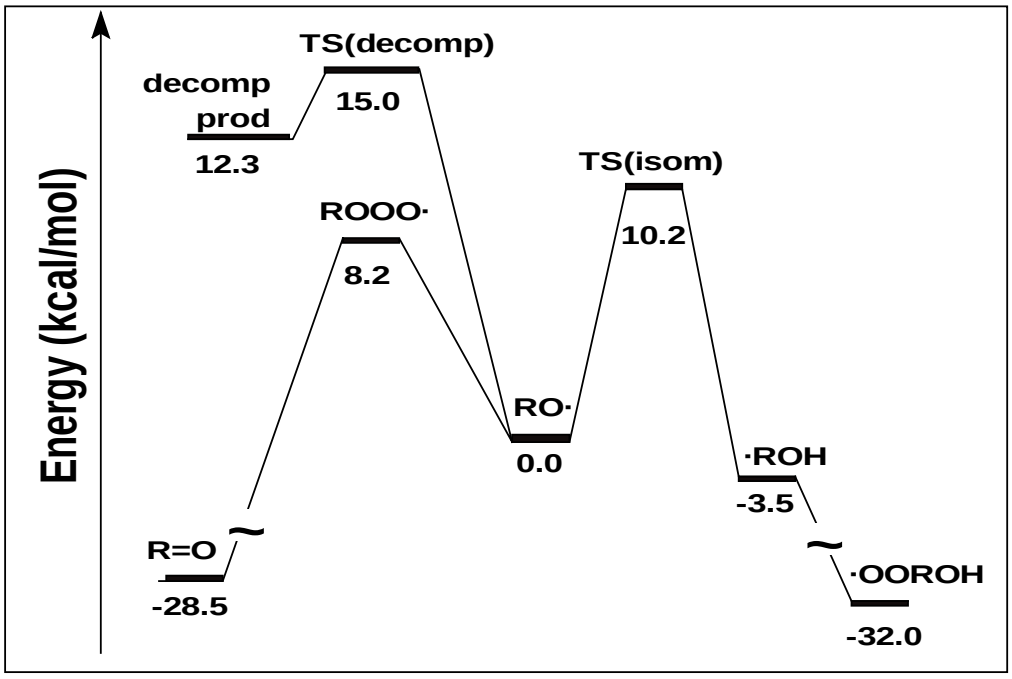

Figure 4.1. Energy diagram for the decomposition (top left), reaction with O_2 (bottom left), and isomerization reactions (right) of *n*-butoxy radicals. Energies for the isomerization and decomposition are taken from Somnitz and Zellner [79, 80] at the modified G2(MP2,SVP) level of theory, while energies for the reaction with O_2 are taken from Jungkamp et al.[81] at the B3LYP/6-311+G(3df,2p)//B3LYP/6-31G(d,p) level of theory. All energies listed are relative to the *n*-butoxy radical.

Only alkoxy radicals that can form a 6-membered ring transition state have a sufficiently low barrier for unimolecular isomerization to be atmospherically relevant [82-86]. The isomerization rate increases when the product is a secondary or tertiary alkyl radical, due to a lowering of the barrier to reaction [82]. Unimolecular decomposition is an available pathway for all alkoxy radicals. Similar to isomerization, the rate of unimolecular decomposition has a strong structural relationship. The rate increases when the transition state is stabilized through substitution at the α- or β-carbon.

The reaction pathways of alkoxy radicals have been the subject of many studies, both experimental and theoretical. Several reviews are available [77, 78, 82, 87-89]. For molecules with all three reaction pathways "open", isomerization and reaction with O_2 dominate under atmospheric conditions. Isomerization has been a particularly difficult process to study experimentally due to the wide range of values of k_{isom} and the fast secondary chemistry. In molecules that cannot form a 6-membered ring, isomerization is too slow to compete with reaction with O_2 or decomposition. In molecules that can form a 6-membered ring, isomerization generally occurs on the timescale of microseconds or less. As opposed to reaction with O_2 or decomposition, isomerization also has no stable product that can be detected long after reaction occurs. As a result, the isomerization of alkoxy radicals has not yet been observed directly. This results in a major uncertainty in the kinetics of alkoxy radicals.

Many previous studies of k_{isom} have focused on the simplest alkoxy radicals that can undergo isomerization: *n*-butoxy and 1- and 2-pentoxy. Under conditions relevant to the lower atmosphere (300K, 1 bar, 21% O_2) the lifetime for reaction with O_2 is on the order of 20 μs. Previous relative rate measurements have estimated the lifetimes for

isomerization under these conditions to be on the order of 5 μs for reaction 4.5 and 3 μs for reaction 4.8. The decomposition reactions have been estimated to occur on longer timescales: on the order of 1 ms for reaction 4.6 and 100 μs for reaction 4.9. As a result, isomerization and reaction with O_2 are expected to be the dominant fates for these alkoxy radicals.

Most previous experimental measurements have been conducted in static smog chambers or slow-flow gas kinetic cells in which the concentration of the end products were measured [83, 85, 86, 90-95]. Alkoxy radicals were produced through generation of the corresponding alkyl radical followed by reactions 4.2-4.3 or by UV photolysis of the corresponding alkyl nitrite. The relative rate constants for isomerization to reaction with O_2 (k_{isom}/k_{O2}) were estimated by measuring the concentrations of end products as a function of oxygen pressure. Often, several reaction pathways can generate the same products, and so it can be difficult to deduce reaction mechanisms by relying on end-product data [81].

In the presence of O_2, the hydroxyalkyl radicals formed in reactions 4.5 and 4.8 rapidly associate with O_2 to form a hydroxy peroxy radical.

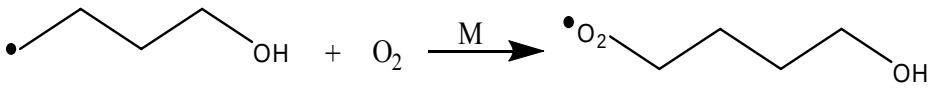

Reaction 4.10

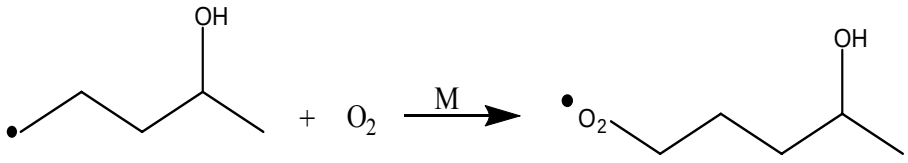

Reaction 4.11

Under lower atmospheric conditions, this association reaction occurs on the order of 50 ns. Most prior experiments have included NO. In this case the products of

reactions 4.10 and 4.11 react with NO via reaction 4.3 to generate a secondary alkoxy radical. This secondary alkoxy radical can also undergo reaction via several pathways, leading to a large variety of possible end-products as well as end products that can be generated by many different pathways. Hein et al. [96] made the only measurement of k_{isom} that did not rely on end product analysis. They measured the secondary production of OH and NO_2 using laser-induced fluorescence and then fit their observed time profiles using a kinetic model. This measurement still relied upon an accurate knowledge of secondary kinetics and was limited to low pressures (P = 50 mbar).

An additional concern in studying the reaction pathways of alkoxy radicals is the possibility of preparing vibrationally excited alkoxy radicals. Hot alkoxy radicals result from excess nitrite photolysis energy or the exothermicity of reaction 4.3. Some of this energy is distributed in the vibrational modes of the alkoxy radicals. Vibrationally hot alkoxy radicals could undergo prompt isomerization (reaction 4.12) or prompt decomposition (reaction 4.13) before becoming thermalized by collisional energy transfer:

$$RCH_2O\bullet^* \rightarrow \bullet RCH_2OH \qquad \text{Reaction 4.12}$$

$$RCH_2O\bullet^* \rightarrow \bullet R' + CH_2O \qquad \text{Reaction 4.13}$$

Two previous experiments have addressed the role of hot alkoxy radicals. Geiger et al. prepared *n*-butoxy radicals from 254 nm photolysis of a *n*-butyl iodide/O_2/NO/N_2 mixture, and noted that their observed oxygen dependence on k_{isom}/k_{O2} was best explained by the presence of 10%-20% hot butoxy radicals [97]. Cassanelli et al. prepared *n*-butoxy radicals by photolyzing *n*-butyl nitrite at 370 ± 10 nm (FWHM) and estimated a 10% yield of product due to nonthermal prompt isomerization [95].

In contrast to previous studies, the experiments described here directly detect the primary isomerization products of *n*-butoxy and 2-pentoxy radicals. Alkoxy radicals were generated through the UV photolysis of the corresponding alkyl nitrites. Product spectra were then taken using infrared cavity ringdown spectroscopy (CRDS). CRDS utilizes a high finesse optical cavity to measure very small absorbances and is an increasingly popular method for monitoring trace species [8, 98, 99]. While other studies have detected products on timescales of minutes to hours after initiating the reaction, our CRDS spectrometer afforded detection of reaction products 10-100 μs after the generation of alkoxy radicals. Additionally, the high sensitivity of CRDS enabled us to work with low concentrations of alkoxy radicals and NO ($[RO]=[NO]\approx10^{14}$ molecules$\times$cm^{-3}). This minimized the generation of secondary alkoxy radicals from reaction 4.3 and possible RO + RO side reactions. As a result, we have been able to make the first direct measurements of the products of alkoxy radical isomerization.

Our measurements were made with a slow-flow cell coupling laser photolysis for the generation of alkoxy radicals and pulsed infrared CRDS for the detection of the OH-stretch band formed from the isomerization reactions 4.5 and 4.8. Since these reactions were too fast for us to measure the isomerization kinetics directly, we measured the relative rate k_{isom}/k_{O2} by measuring the primary isomerization product concentration as a function of O_2 concentration. The measurement of products on short timescales has also allowed us to evaluate the role of prompt unimolecular reactions in our system.

4.2 Experimental Methods

These experiments were the continuation of a project started by Eva Garland. The general experimental method used in the experiments described here was the same as for the first generation of experiments described in her thesis [20]. The main challenge found in her early work was poor signal to noise due to low photolysis yields and large background due to photolysis precursors. We have made improvements in these areas through a more powerful excimer and a new photolysis cell designed to minimize dead volume and UV scatter.

Our experimental setup consisted of a slow-flow cell in which alkyl nitrite precursors were photolyzed with an excimer laser to generate alkoxy radicals. These experiments were performed at a pressure of 670 torr, with mixtures of O_2 and N_2 used as bath gases. The experimental repetition rate was 10 Hz, and the gas mixture was flushed through the cell every 70 ms, so that a fresh gas sample was probed with each laser pulse.

The reaction products were probed with IR-CRDS. Pulsed infrared radiation was generated with an optical parametric amplifier (OPA) at the difference frequency between the outputs of a doubled YAG (532 nm) and a tunable dye laser (approximately 630 nm). The time between the photolysis and the detection was varied from 0 to 100 μs in order to obtain the time profile of product formation. The time resolution of the detection was limited by the ringdown time. Approximately 40 μs of the ringdown curve were used to generate an exponential fit for which the 1/*e* time was approximately 3-5 μs. Spectra were collected by averaging 16 shots with the excimer on and then 16 shots with the excimer off at each wavelength. The signal with the excimer off (no alkoxy radical

formation) was subtracted to eliminate background from precursor gases and changing mirror reflectivity.

We employed this setup to measure the infrared spectra of alkoxy radical reaction products. Spectra were recorded from 3400 to 3700 cm^{-1}, and the OH stretch in this region was used to identify the products from the isomerization pathway. As shown in reactions 4.4-4.11, isomerization is the only pathway of alkoxy radicals that is expected to yield products containing a hydroxyl group. The observed OH stretch peak was also monitored as a function of O_2 concentration to measure the rate of isomerization of alkoxy radicals relative to the rate of their reaction with O_2, k_{isom}/k_{O2}.

4.2.1 Generation of Alkoxy Radicals

Alkoxy radicals were generated *in situ* from their nitrite precursors with the output beam from an excimer laser (Lambda Physik LPX 200) at either 254 nm or 351 nm:

$$RONO + h\nu \rightarrow RO\bullet + NO. \qquad \text{Reaction 4.14}$$

Alkyl nitrites were introduced to the cell by bubbling nitrogen through a bubbler kept at 0 ^{o}C. The concentration of alkyl nitrites was determined by an absorption measurement of the helium/alkoxy nitrite flow at 254 nm. The cross section of methyl nitrite at 254 nm is 1×10^{-18} cm^2, and the cross section for the other alkyl nitrites is expected to be similar. Alkyl nitrite concentrations in the reaction cell were kept as low as possible (on the order of 10^{16} cm^{-3}) to minimize spectral interference from their broad absorption of infrared radiation in the 3300-3750 cm^{-1} range.

The butyl nitrite precursors were purchased from Aldrich (95% purity). 2-pentyl nitrite was synthesized from pentanol in aqueous sodium nitrite, using a modification of the synthesis of 1-butyl nitrite described in *Organic Syntheses vol. 2* [100]. Briefly, a cold mixture of sulfuric acid and 2-pentanol was added slowly to a cold aqueous solution of sodium nitrite. The crude product was distilled to reduce the amount of excess residual pentanol. Based on FTIR spectra of the distilled 2-pentyl nitrite, the ratio of 2-pentyl nitrite to 2-pentanol was 8/1. Nitrogen and oxygen were used as bath gases, and the relative ratios of these gases in the reaction cell were used in the determination of the ratio of k_5/k_4. Gas flow rates were measured with mass flowmeters (Omega, Edwards) calibrated volumetrically. Gases were mixed in a glass cross 5 cm upstream from the photolysis region. Typical experimental conditions are listed in Table 4.1.

Table 4.1. Typical experimental conditions for alkoxy radical isomerization studies.

N_2 Purge Flow–Left Mirror	650 sccm
N_2 Purge Flow–Right Mirror	650 sccm
N_2 Bubbler Flow	225 sccm
N_2 Dilution Flow	0–6000 sccm[a]
O_2 Dilution Flow	0–6000 sccm[a]
Cell Pressure	670 torr
Temperature	295 K
Residence Time	70 ms
Optical Cell Length	55 cm
Photolysis Window Length	6 cm
Excimer Energy at 351 nm	200 mJ/pulse
$\Delta\tau/\tau$	0.4%

a The sum of the N_2 and O_2 dilution flows was kept constant at 6000 sccm.

Most experiments were performed while operating the excimer laser at 351 nm. At this wavelength, the typical output energy was 200 mJ / pulse. The output beam, initially 3 cm × 1 cm, was focused vertically and expanded radially so that the resulting

beam at the cell was 6 cm × 0.3 cm, collimated in the vertical axis and slightly divergent horizontally. The flux of photons entering the cell was 1.0×10^{17} photons cm^{-2} resulting in approximately 1% photolysis of the nitrite precursors ($\sigma_{351} = 8 \times 10^{-20}$ cm^2).

Experiments with the excimer laser operating at 248 nm were performed previously by Eva. For these experiments, the output beam was focused vertically and expanded radially so that the resulting beam at the cell was 10 cm × 0.5 cm. The typical output energy was 125 mJ / pulse, resulting in approximately 5% photolysis of the nitrite precursors ($\sigma_{351} = 1.3 \times 10^{-18}$ cm^2) [20].

The timing of the excimer and YAG lasers was controlled by digital delay generators (SRS model DG535 and EG&G Princeton Research Model 9650). This set the time delay between the preparation of reactants (via photolysis) and the detection of products with cavity ringdown spectroscopy. Data were collected in two modes: frequency spectra were obtained by holding the photolysis-probe delay fixed (typically at 100 μs) and scanning in frequency space, while kinetics scans were obtained by holding the IR wavelength fixed and varying the photolysis-probe delay. In both cases ringdown traces were collected at each point with the excimer on and with the excimer off. The frequency-dependent background of precursor gases and mirror reflectivity could then be subtracted.

4.2.2 CRDS Detection

A schematic of the apparatus is shown in Figure 4.2. The gas kinetics cell consisted of a 7 cm × 1 cm metal rectangular tube, coated with a fluoropolymer (FluoroPel PFC 801A/coFS) to minimize reactions at the walls. Fused silica windows of

6 cm length were placed on two sides of the cell to allow light from an excimer laser to pass through. The cell was coupled to ringdown mirrors via Teflon blocks containing ports for introducing reactant gases and measuring the cell pressure. For gas flow cell dimensions and assembly details see appendix B.

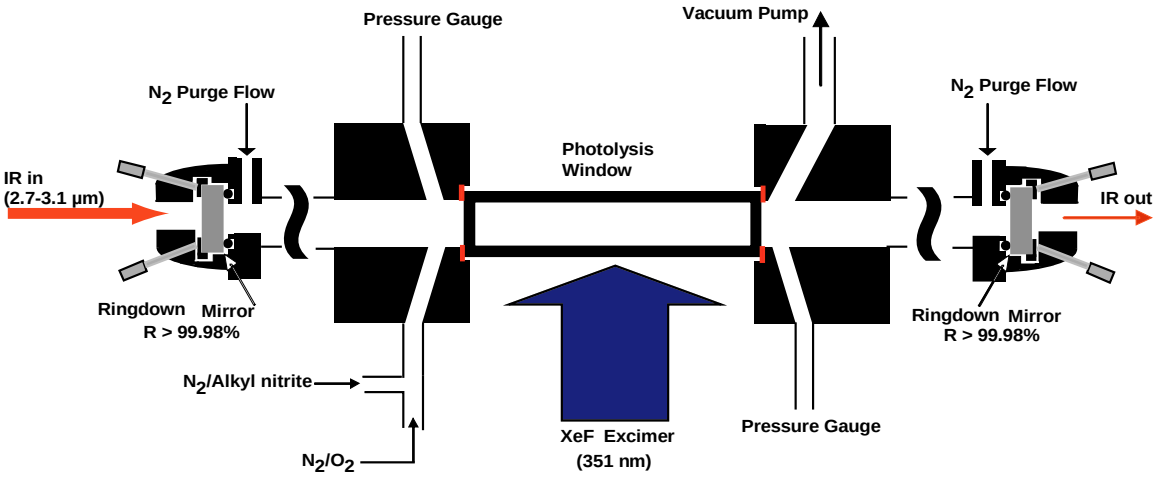

Figure 4.2. Diagram of the UV photolysis / gas kinetics cell. Experiments were conducted at 670 torr and 295 K. Typical residence time for the gases was 70 ms.

Details of the cavity ringdown apparatus are given in Chapter 1. For these experiments, the purge volume consisted of 24-cm long glass tubes connected to the ringdown mirror mounts and the Teflon blocks via Ultra-torr adapters. Ringdown data were collected for 40 μs after the Nd:YAG laser fired, at a rate of 50 MSa s^{-1}. Ringdown traces from 16 shots were averaged and then fit to an exponential decay using a Levenberg-Marquardt algorithm. Typical background ringdown times were on the order of 7 μs. The standard deviation of successive ringdown times obtained for an empty cell was typically 0.4%, giving a minimum detectable absorbance of 2.6 ppm per pass $Hz^{-½}$. In the presence of the alkyl nitrite precursor, typical ringdown times were on the order of

3 μs. The standard deviation of successive ringdown times was typically 0.4%, giving a minimum detectable absorbance of 6.1 ppm per pass $Hz^{-½}$.

4.2.3 Relative Kinetics Measurements

We have measured an absorption feature in the infrared we attribute to the initial product of isomerization. We have used this spectral feature to measure the relative rate of isomerization to reaction with O_2 at 298 K. This was accomplished by measuring the decrease in the absorbance of this feature as a function of O_2. From this, k_{isom}/k_{O2} was derived.

4.3 Results

4.3.1 Chemistry

Photolysis of the alkyl nitrites in the UV leads to prompt dissociation on the excited state surface.

$$RONO + h\nu \rightarrow RO\bullet + NO\bullet \qquad \text{Reaction 4.14}$$

The nascent products RO• and NO• appear on timescales of <1ps. At the laser fluences used at 351 nm, we expect $[RO\bullet] \approx 2\times10^{14}$ molecules×cm^{-3} (~1% photolysis of the precursors). Based on rate constants from the literature, isomerization for *n*-butoxy and 2-pentoxy radicals occurs on time scales of ~5 μs and ~2 μs, respectively [82],

$$RO\bullet \rightarrow HOR\bullet\ , \qquad \text{Reactions 4.5, 4.8}$$

while decomposition occurs on time scales of ~50 ms. At the low concentrations used, recombination reactions of RO• with NO• or RO• ,

$$RO\bullet + RO\bullet \rightarrow ROOR, \text{ other products}, \qquad \text{Reaction 4.15}$$

$$RO\bullet + NO\bullet \rightarrow RONO, \qquad \text{Reaction 4.16}$$

are approximately two orders of magnitude slower than isomerization. Thus, isomerization or the competing reaction with O_2 to form HO_2 and the respective aldyehyde or ketone will be the dominant fate of the alkoxy radicals. The next question is then the identity of the observed bands.

In the absence of O_2 the fate of the isomerization products, the hydroxy-alkyl radicals HOR•, is either recombination with NO• or self-association.

$$HOR\bullet + HOR\bullet \rightarrow (HOR)_2 \qquad \text{Reaction 4.17}$$

$$HOR\bullet + NO\bullet \rightarrow HORNO \qquad \text{Reaction 4.18}$$

If we assume that the HOR• + HOR• association reactions are in the high pressure limit with a gas kinetic rate constant 2×10^{-11} cm^3s^{-1}, then the initial lifetime is 130 μs. At 100 μs, approximately 50% of the HOR• radicals will have recombined. The high pressure rate coefficient for association with NO is expected to be approximately 3×10^{-12} cm^3s^{-1}. Thus, at 100 μs approximately 50% of the observed OH signal will come from HOR• monomers, with the remainder having dimerized to form a 1,8-octyl diol. Less than 4% as RONO and a similar small percentage may have undergone hydrogen abstraction to form butanol and a hydroxy-butene. We therefore assign these peaks both to the δ-hydroxy alkyl radicals and to their immediate reaction products.

In the presence of O_2, the hydroxyl-alkyl radicals HOR• will associate to form peroxy radicals HOROO• with a rate coefficient of roughly 7×10^{-12} cm^3s^{-1} [36],

$$HOR\bullet + O_2 + M \rightarrow HOROO\bullet , \qquad \text{Reaction 4.2}$$

although there is probably a minor channel to form HO_2 and a hydroxylated alkene. At 1 torr of O_2, the pseudo-first-order lifetime is 5 μs. Assuming that the rate constant for the

HOROO• self reaction is comparable to that for *n*-$C_4H_9O_2$ self-reaction (4×10^{-13} cm^3 s^{-1} [101]), no appreciable reaction will occur in less than 1 ms. For all but the lowest O_2 pressures used in this experiment, all spectra observed at 100 μs in the presence of O_2 will be those of the hydroxyl peroxyl radicals.

4.3.2 Spectra

Figure 4.3 shows a series of infrared spectra obtained following the photolysis of alkyl nitrite precursors. All spectra shown were taken with a photolysis-probe delay of 100 μs and have had the background signal in the absence of photolysis subtracted. We see that the nitrite precursors and contaminants therein contributed significant background, roughly 10 times the signal due to products. This background was much worse for our synthesized 2-pentyl nitrite, presumably due to larger contamination due to remaining pentanol. We see that the signal to noise was much better for the n-butyl nitrite photolysis, but that in both cases a peak can be clearly distinguished in the OH stretch region. Spectra were collected while varying the photolysis-probe delay from 5 μs to 100 μs, and in all cases the spectra were identical, indicating that all peaks appear promptly, on timescales shorter than the time resolution of our experiment (5 μs). As a result, the observed features are all due to the alkoxy radicals or their immediate reaction products.

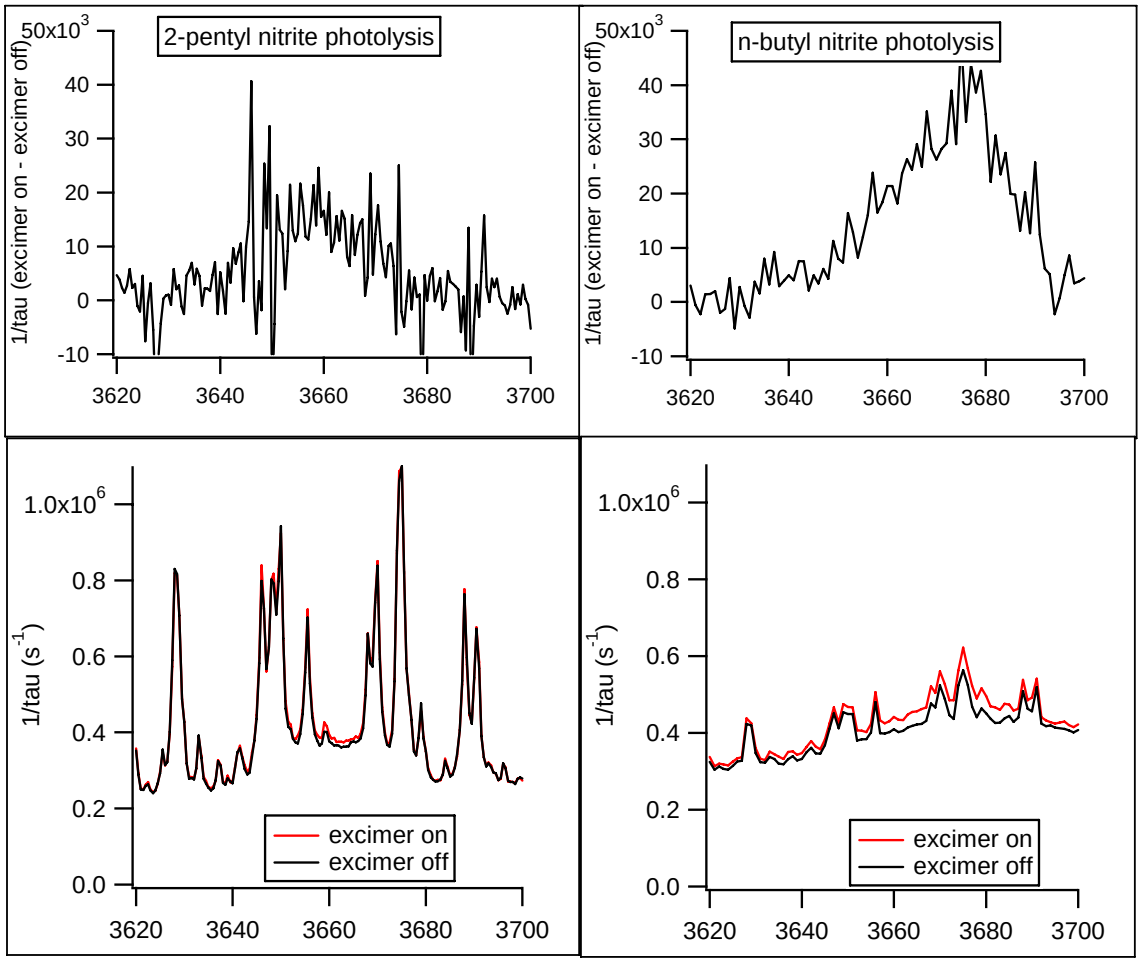

Figure 4.3. Representative CRDS spectra of products formed 100 μs after photolysis. Raw data with and without the excimer photolysis are shown on the bottom while the top shows the subtraction of the two.

An attempt was made to maximize the signal to noise by reducing precursor concentrations and increasing the UV flux. This was beneficial to a point, but eventually resulted in unintended negative consequences. Figure 4.4 shows the peak signal following n-butyl nitrite photolysis as a function of photolysis-probe delay. Standard time profiles are shown on the left. On the right are time profiles taken with the photolysis beam focused tightly to increase photon flux. While the peak signal appeared to be larger with the focused excimer, we also saw very large time-dependent peaks in the

signal. These peaks were shown to be independent of frequency and were attributed to photoaccoustic destabilization of the optical cavity. Following the observation of these photoaccoustic peaks, the photolysis cell was found to have black soot on the walls coincident with the transmission path of the excimer. Subsequent experiments were conducted with a more diffuse excimer beam to prevent this "burning" of the nitrites onto the windows.

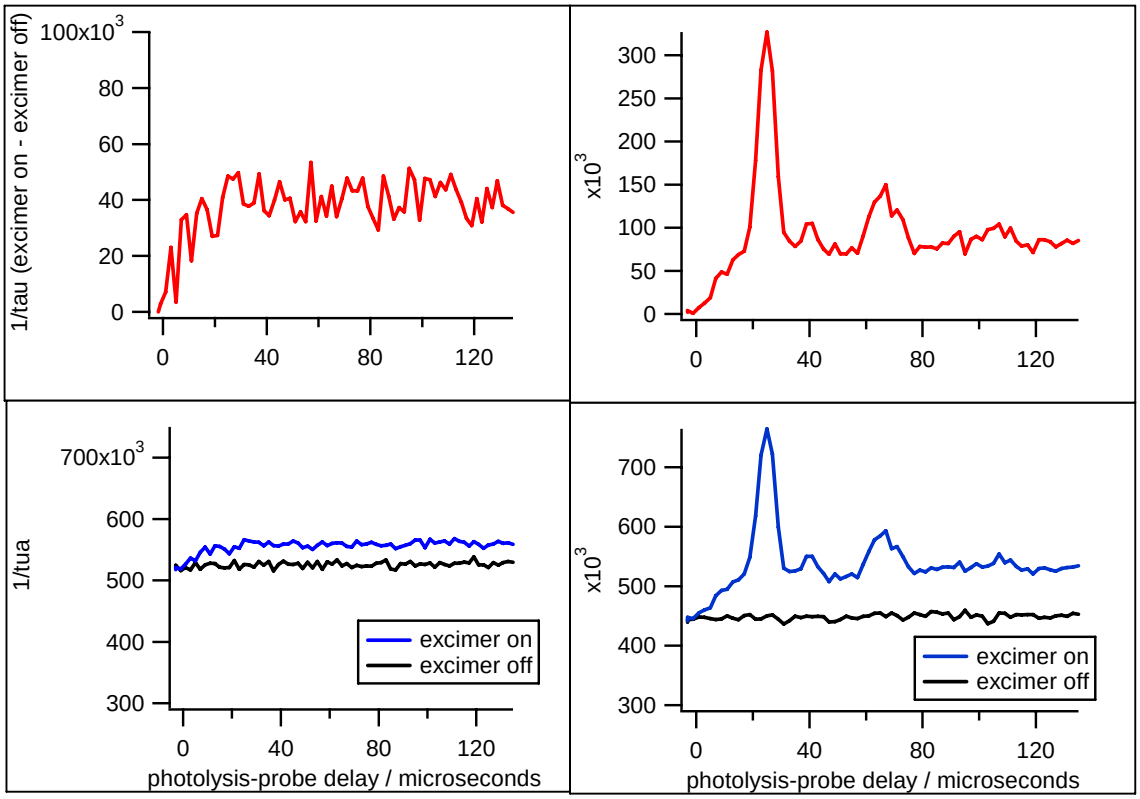

Figure 4.4. CRDS signals at 3680 cm^{-1} as a function of photolysis-probe delay. The left two panels were taken using our standard UV beam profile. The right two panels were taken with the UV profile focused tightly in the vertical direction.

Figure 4.5, Figure 4.6, and Figure 4.7 all show the average of many spectra in this region to improve the signal to noise. Figure 4.5 shows the IR spectra of products formed following the generation of four different alkoxy radicals: *n*-butoxy, 2-pentoxy, isobutoxy, and *tert*-butoxy. All radicals were produced from photolysis of the

corresponding alkyl nitrites at 351 nm in the absence of O_2. Following photolysis of *n*-butyl nitrite and 2-pentyl nitrite, a clear peak is observed in the OH-stretch region at 3675 cm^{-1}. This peak does not appear following the photolysis of isobutyl nitrite or *tert*-butyl nitrite.

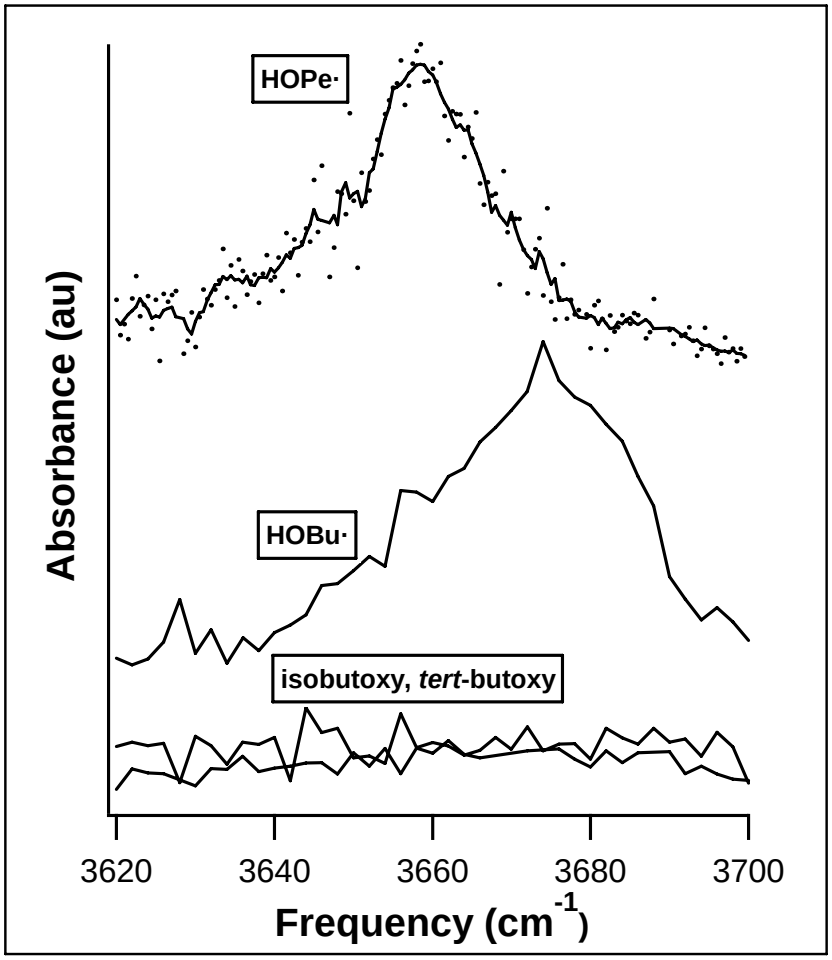

Figure 4.5. OH stretch infrared spectra of the isomerization products of 2-pentoxy (δ-hydroxy-*n*-pentyl, top) and of *n*-butoxy (δ-hydroxy-*n*-butyl, middle). The product spectra following the generation of isobutoxy and *tert*-butoxy radicals (bottom) show no absorption features above our background noise.

The shapes and positions of the peaks observed from *n*-butoxy and 2-pentoxy products are nearly identical to the OH-stretch bands found in the infrared spectra of *n*-butanol and 2-pentanol, respectively (Figure 4.6). As expected, we only observe the

alcohol OH-stretches from alkoxy radicals that are long enough to undergo a 1,5-hydrogen shift, and these peaks appear on the very fast timescales we would expect for unimolecular isomerization. Using literature values for k_{isom}/k_{O2} and taking the OH absorption cross section of the isomerization products to be equivalent to *n*-butanol (7.5×10^{-20} cm^{-2}) [102] we estimate that the concentration of OH-containing isomerization products was approximately 1.5×10^{14} molecules$\times cm^{-3}$. This is consistent with our estimate of the nitrite photolysis yield.

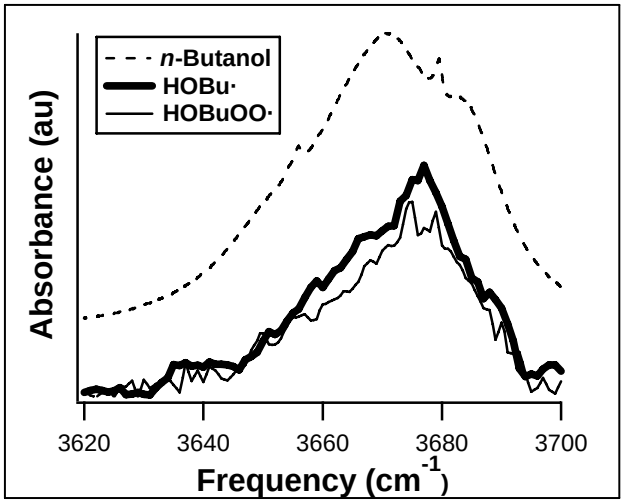

Figure 4.6. Hydroxy stretch infrared spectra of *n*-butanol (top), the butoxy isomerization product (δ-hydroxy-*n*-butyl, middle), and the butoxy isomerization product in the presence of $[O_2] = 1\times10^{19}$ molecules$\times cm^{-3}$ (δ-hydroxy-*n*-butyl peroxy, bottom).

Figure 4.6 compares three spectra: the photolysis products of *n*-butyl nitrite in the absence of O_2, the photolysis products of *n*-butyl nitrite in the presence of O_2, and the IR spectrum of butanol [103]. At our O_2 concentrations ($[O_2] = 1\times10^{19}$ molecules$\times cm^{-3}$), the initial δ-hydroxy-*n*-butyl isomerization product will associate with O_2 faster than the detection time of our experiment. We therefore assign the peak at 3675 cm^{-1} in the

presence of O_2 to the δ-hydroxybutyl peroxy radical. We see that the presence of the peroxy group has minimal impact on the shape or position of the OH stretch band.

4.3.3 Prompt Isomerization and Decomposition

Figure 4.7 shows the IR spectrum of products formed following the photolysis of *n*-butyl nitrite at two UV wavelengths: 248 nm and 351 nm. In addition to the OH stretch peak, a second absorption feature is observed in the spectrum taken following photolysis at 248 nm. The feature centered at 3565 cm^{-1} matches the position and band shape of the $2\nu_2$ band of formaldehyde, one of the products of unimolecular decomposition. Assuming a δ-hydroxy-*n*-butyl cross section similar to that of *n*-butanol, we estimate a 60% yield of decomposition upon photolysis at 248 nm. The observation of a significant decomposition yield was not expected based on estimates of the thermal rate constants. The photolysis spectrum obtained following 351 nm photolysis shows no evidence of formaldehyde. For typical experimental conditions, the minimum detectable limit for HCHO is 7×10^{12} molecules×cm^{-3}. Since typical values of $[C_4H_9O]$ were 2×10^{14} molecules×cm^{-3}, an upper limit of 5% of butoxy radicals undergo dissociation when butyl nitrite is photolyzed with 351 nm radiation. We therefore believe this formaldehyde is evidence of nonthermal (prompt) decomposition of *n*-butoxy radicals formed with a large amount of internal energy following photolysis at 248 nm.

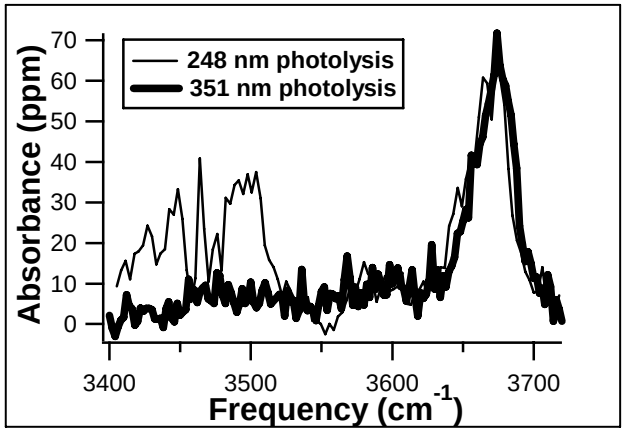

Figure 4.7. Infrared spectra of the photolysis products of *n*-butyl nitrite at 248 nm and 351 nm. The peak at 3470 cm^{-1} is assigned to formaldehyde, formed through prompt decomposition of the alkoxy radicals when generated through photolysis at 248 nm.

While we see no evidence of prompt decomposition at 351 nm, it is still possible that prompt isomerization occurs, since the barrier for isomerization is calculated to be 5 kcal mol^{-1} lower than that for decomposition [79, 80]. Since both prompt and thermal isomerization are expected to occur on timescales faster than our kinetic resolution, there is no direct method for us to measure the amount of prompt isomerization. However, if a significant fraction of our isomerization product was formed nonthermally, we would expect that to impact our relative rate measurement, as will be discussed in the next section. In order to minimize the impact of prompt unimolecular processes on our relative rate measurements, all kinetics data were taken using 351 nm as the photolysis wavelength.

4.3.4 Relative-Rate Measurements

Attempts to measure the δ-hydroxy-*n*-butyl and δ-hydroxy-*n*-pentyl formation kinetics revealed that the isomerization occurred faster than the time resolution of our apparatus, yielding a lower limit for k_{isom} of 2×10^5 s^{-1}. We therefore measure the rate of

unimolecular isomerization relative to the rate of reaction with oxygen, k_{isom} / k_{O2} by measuring the yield of isomerization product as a function of oxygen concentration. By using the steady state approximation (assuming that $k_{decomp} << k_{isom}$) and solving for 1/[ROH], it can be shown that

$$\frac{1}{[ROH]} = \frac{k_{O_2}[O_2]}{k_{isom}[RO]} + \frac{1}{[RO]}. \qquad \text{Equation 4.1}$$

[ROH] is the concentration of isomerization product, [RO] is the concentration of alkoxy radicals and $[O_2]$ is the oxygen concentration. The branching ratio k_{isom}/k_{O2} can be obtained by plotting 1/[ROH] vs. $[O_2]$ and taking the ratio of the intercept to the slope.

Data were taken by varying $[O_2]$ and rapidly scanning (3620-3700 cm^{-1} at 0.5 cm^{-1} steps) over the OH stretch peak. [ROH] was then obtained by fitting each spectrum to a previously obtained reference spectrum (10 averaged scans, 0.5 cm^{-1} step size) and estimating [ROH] from the height of the peak at 3675 cm^{-1}. Data taken in sets of seven to ten O_2 concentrations were analyzed separately to minimize the impact of long-term drift in precursor concentrations or laser fluence upon our k_{isom}/k_{O2} determinations. Multiple sets of data (14 sets for *n*-butoxy, 5 sets for 2-pentoxy) were obtained and analyzed according to the aforementioned procedure. Plots of 1/[ROH] vs. $[O_2]$ for *n*-butoxy and 2-pentoxy taken at 670 torr are shown in Figure 4.8 and Figure 4.9. At high oxygen concentrations, [HOR] decreased linearly as $[O_2]$ increased, consistent with the competition of the isomerization and O_2 reaction pathways.

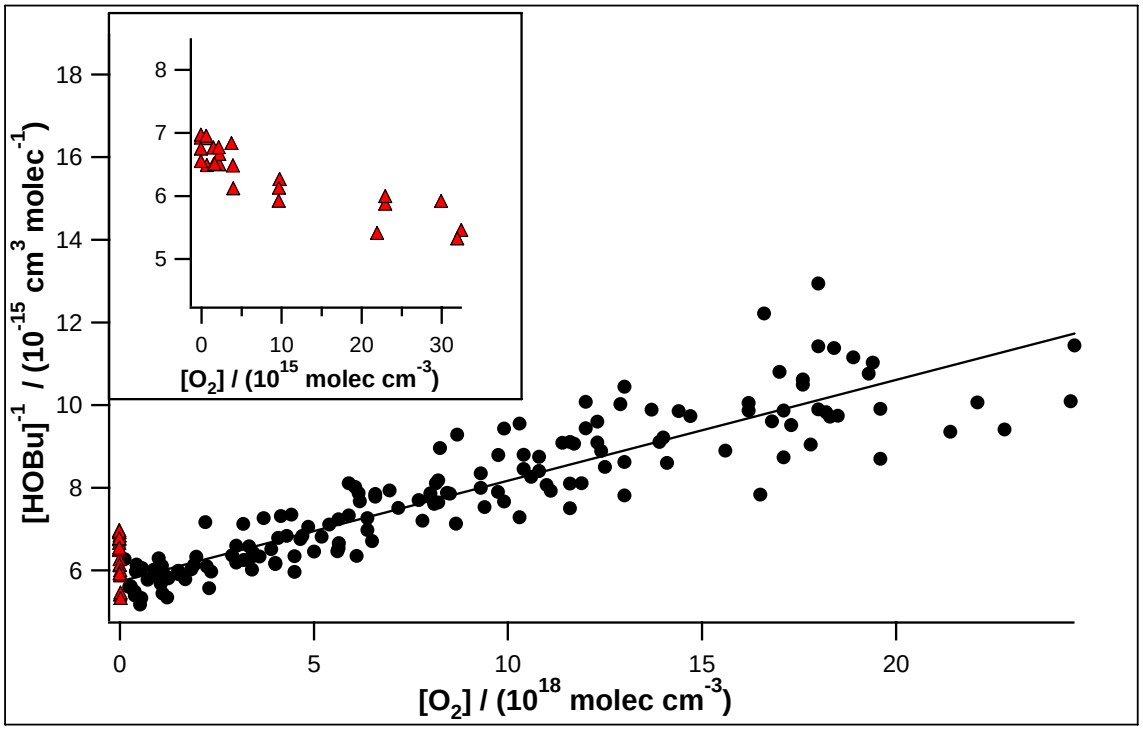

Figure 4.8. Measurements of 1/[HOROO•] plotted as a function of [O_2] for *n*-butoxy. [HOROO•] were calculated from the strength of the OH-stretch infrared peak. Individual data sets have been scaled to [*n*-butoxy] = 2×10^{14} molecules×cm^{-3} at [O_2] = 0. Data above [O_2]=1×10^{17} cm^{-3} show the expected decrease in [HOROO•] with [O_2]. The inset shows an apparent decrease in [$HOC_4H_8OO\cdot$] with [O_2] at very low [O_2] as discussed in the text. Only the data with [O_2] > 5×10^{16} molecules×cm^{-3} were used in the linear fit to determine k_{isom}/k_{O2}. Slope = $(2.4 \pm 0.2) \times 10^{-34}$ cm^6, intercept = $(5.7 \pm 0.2) \times 10^{-15}$ cm^3, $k_{isom}/k_{O2} = (2.3 \pm 0.2) \times 10^{19}$ cm^{-3}. All errors are reported to 2σ.

Data taken at very low oxygen concentration (shown as an inset to Figure 4.8) exhibited anomalous behavior; The apparent [HOR] decreased with lower [O_2]. At [O_2] < 5×10^{16} cm^{-3} the lifetime for this addition becomes comparable to our detection time. This anomalous behavior is therefore likely related to the addition of O_2 to the initially formed hydroxyalkyl radicals. One possible explanation is that the apparent decrease in [HOR] is due to a change in the OH stretch cross section in the presence of the peroxy group. An increase of only ≈ 10% in the cross section upon addition of the peroxy group would be required to explain our data. An alternate explanation for our data could be

that, if the initially formed hydroxyalkyl radicals are not rapidly converted to the hydroxyalkyl peroxy radicals, a small fraction re-isomerize back to the alkoxy radical. Calculations on the energetics of *n*-butoxy reactions (Figure 4.1) indicate that the isomerization channel is only slightly exothermic. Using Somnitz and Zellner's calculated ΔH_{isom} for *n*-butoxy (-3.4 kcal mol^{-1}) [79], the ratio of isomerization product to remaining alkoxy [·ROH]/[RO·] is 311.

Regardless of the mechanism, an accurate value of k_{isom}/k_{O2} should be obtained when $[O_2]$ is high enough to ensure rapid conversion of hydroxyalkyl radicals to hydroxyalkylperoxy radicals. As a result, only data with $[O_2] > 5\times10^{17}$ cm^{-3} were used to determine k_{isom}/k_{O2}. Each set was normalized to an initial alkoxy radical concentration of 2×10^{14} cm^{-3} and then fit using a linear least squares regression. The fits obtained in this way were not statistically different than if the sets were fit individually and then averaged. Because prompt isomerization will increase the value of k_{isom}/k_{O2}, this leads to asymmetric error bars. Thus, the results we report are $k_{isom}/k_{O2} = 2.3(+0.2, -0.5) \times 10^{19}$ for *n*-butoxy, and $k_{isom}/k_{O2} = 3.3(+0.4, -0.7) \times 10^{19}$ for 2-pentoxy. All errors are stated to 2σ, and the increased uncertainty for 2-pentoxy stems from the smaller number of data sets.

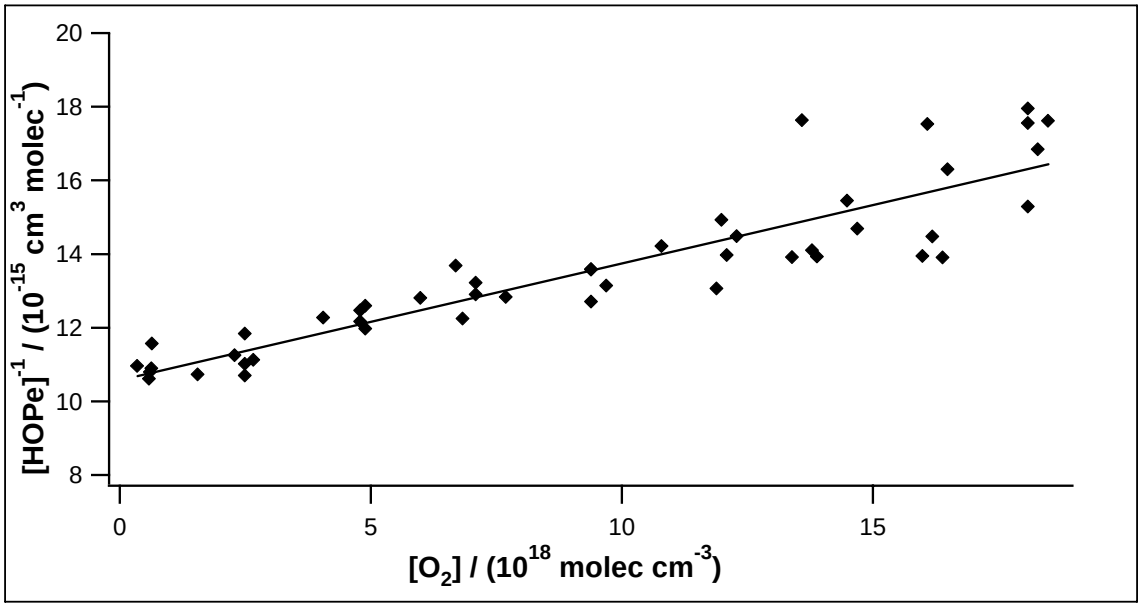

Figure 4.9. Measurements of 1/[HOROO•] plotted as a function of [O_2] for 2-pentoxy. [HOROO•] were calculated from the strength of the OH-stretch infrared peak. Individual data sets have been scaled to [2-pentoxy] = 1×10^{14} molecules×cm^{-3} at [O_2] = 0. Slope = $(3.2 \pm 0.2) \times 10^{-34}$ cm^6, intercept = $(1.06 \pm 0.02) \times 10^{-14}$ cm^3, $k_{isom}/k_{O2} = (3.3 \pm 0.4) \times 10^{19}$ cm^{-3}. All errors are reported to 2σ.

Several data sets were taken replacing all N_2 with Ar to observe the impact of the collision partner. The Ar data sets resulted in values of k_{isom}/k_{O2} that were statistically indistinguishable from the N_2 data, indicating that 670 torr lies near the high-pressure limit of the termolecular falloff curve in agreement with RRKM calculations [104].

We can now re-evaluate the possible influence of prompt isomerization on these measurements. When the possibility of prompt isomerizaiton is included in eq 4.1, the expression for [C_4H_8OH] becomes

$$\frac{1}{[ROH]_{tot}} = \frac{k_{O_2}[O_2] + k_{isom}}{k_{isom}\left([RO] + [ROH]_p\right) + k_{O_2}[O_2][ROH]_p}, \qquad \text{Equation 4.2}$$

where $[ROH]_p$ is the amount of product formed through the prompt isomerization channel.

We see from eq 4.2 that a significant yield of prompt isomerization product would lead to a nonlinear dependence of 1/[•ROH] on [O_2]. This provides a method for us to quantify the extent of prompt isomerization. We first assumed no prompt isomerization in order to determine the ratio k_{isom}/k_{O2} as described above. Using a literature value for k_{O2} of 1×10^{-14} cm^3 molecule^{-1} s^{-1}, we calculate k_{isom} [82]. The value of the intercept from our data plot was used as 1/[RO]. We then compared the residual sum of squares (RSS) for our linear fit to the RSS of a fit using eq 4.2 for various values of $[ROH]_p$. An upper bound on the amount of prompt isomerization was estimated by the value of $[ROH]_p$ that led to a doubling of the linear fit RSS. Based on this analysis, $[ROH]_p < 0.07 \times [ROH]_{total}$ for *n*-butoxy, and $[ROH]_p < 0.05 \times [ROH]_{total}$ for 2-pentoxy. This translates to a possible systematic overestimation of k_{isom}/k_{O2} of 0.3×10^{19} for *n*-butoxy, and 0.3×10^{19} for 2-pentoxy due to prompt isomerization, or a 15% error.

4.4 Discussion

We have made the first observation of the hydroxylated isomerization products of *n*-butoxy and 2-pentoxy radicals. The observed spectra are likely due to a mixture of the initial hydroxyl alkyl radical, the hydroxyl peroxy radical formed from addition of O_2 and some secondary OH-containing species. Nevertheless, the size of the OH peak can be used as a proxy for the isomerization yield. By measuring the variation in the peak magnitude as a function of O_2 concentration, we have measured the relative rate k_{isom}/k_{O2}. Our values for k_{isom}/k_{O2} are compared with previous measurements in Table 4.2. Our measurements are unique in the literature in that they directly probe the isomerization

products microseconds after their formation, minimizing possible interference from secondary chemistry.

Table 4.2. Comparison of k_{isom}/k_{O2} for *n*-butoxy and 2-pentoxy to previous measurements

	k_{isom}/k_{O2} (10^{19} cm^{-3})[a]	Molecule Detected	Method	*p* (torr)	Ref
***n*-butoxy**	**2.3 (+0.2/-0.5)**	**δ-hydroxy-*n*-butyl peroxy**	**slow flow, CRDS**	**670**	**This work**
	1.95 ± 0.4	butanal and 4-hydroxy butanal	static, FTIR	700	Cassanelli, 2006 [94]
	1.5 ± 0.5	butanal	static, GC	760	Cox, 1981 [91]
	1.9 ± 0.4	butanal	static, FTIR	700	Niki,1981 [86]
	2.1 ± 0.5	butanal	slow Flow, GC	760	Cassanelli, 2005 [95]
	1.8 ± 1.1	butanal	slow Flow, GC	760	Cassanelli, 2005 [95]
	0.25 ± 0.19	OH and NO2	fast flow, LIF	38	Hein, 1999 [96]
	1.8 ± 0.6	butanal	static, FTIR	760	Geiger, 2002 [97]
2-pentoxy	**3.3 (+0.4/-0.7)**	**δ-hydroxy-*n*-pentyl peroxy**	**slow flow, CRDS**	**670**	**This work**
	3.1[b]	2-pentone	static, GC	700	Atkinson, 1995 [83]

a All uncertainties are 2σ b Uncertainty is a factor of 2

Previous experimental studies of the *n*-butoxy radical at 1 atm have obtained values for k_{isom}/k_{O2} ranging from 1.5×10^{19} to 2.2×10^{19} cm^3 molec^{-1} [86, 90, 91, 94-96]. A recent report on "Evaluated kinetic and photochemical data for atmospheric chemistry" reports a preferred value of 2.1×10^{19} for k_{isom}/k_{O2} at 298 K and 1 bar pressure, assuming k_{O2} of 1.4×10^{-14} cm^3 molec^{-1} s^{-1} [88].

Our measured value for k_{isom}/k_{O2} is approximately 50% larger for 2-pentoxy radicals than for the *n*-butoxy radicals. This is in agreement with the lower barriers for isomerization of the 2-pentoxy radical seen in calculations [80]. We are only aware of one previous measurement of the 2-pentoxy isomerization kinetics in which Atkinson et al. measured the end products from the photo-oxidation of pentane in a smog chamber

[83]. Their product analysis was complicated by the presence of all three possible pentoxy radicals, resulting in a reported uncertainty of a factor of two. Our measured k_{isom}/k_{O2} is consistent with Atkinson et al., but has much smaller error bars.